Polyhedron 82 (2014) 37–49

Contents lists available at ScienceDirect

Polyhedron

journal homepage: www.elsevier.com/locate/poly

Ruthenium complexes with tridentate ligands for dye-sensitized solar cells

Thomas W. Rees, Etienne Baranoff*

School of Chemistry, University of Birmingham, Edgbaston, B15 2TT Birmingham, UK

ARTICLE INFO

Article history:
Received 25 February 2014
Accepted 26 April 2014
Available online 9 May 2014

Keywords:
Ruthenium complex
Tridentate ligand
Polypyridine
Dye-sensitized solar cell
Photovoltaic

ABSTRACT

Since the first report of black dye, ruthenium complexes with tridentate ligands have attracted attention due to their ability to harvest photons in the near infrared. Herein we review this family of sensitizers for dye-sensitized solar cell focusing on their chemical structures and properties. We briefly highlight their performance in photovoltaic devices.

1. Introduction

Our society consumes approximately 18 terajoules of energy per second, about 100 times the amount utilized a century ago. During this period, the availability of cheap energy from fossil fuels has supported a phenomenal development in technology and, overall, has resulted in a significant improvement of our quality of life, if only from a material point of view.

Unfortunately fossil fuels are becoming more expensive and our rate of energy consumption continues to increase due to growing population and rising demand from developing countries. One of the biggest challenges faced by our society is therefore to replace fossil fuels with a vast, renewable, and affordable energy source while keeping pace with the world's rapidly increasing energy requirements. Furthermore, this challenge has to be answered with an economically and energetically low-cost solution using abundantly available and safe raw materials.

The sun is a particularly attractive source of energy. Nearly 89 petajoules of solar energy reach the Earth's surface every second which amounts to 4000 times our current energy consumption. As a result, the challenge of converting sunlight into electricity, photovoltaics, continues to be a very active topic in research.

Commercially available photovoltaic technologies are based on inorganic materials, the processing of which requires high costs and is highly energy consumptive. Furthermore, many of those materials can be toxic and have a low natural abundance. Organic photovoltaics do not have such issues as the materials are based mainly on carbon and hydrogen atoms, meaning they can easily be disposed of. However, the efficiencies of organic-based photovoltaic cells are a long way behind those obtained by their purely inorganic counterparts.

Conventional organic photovoltaic devices are based on a heterojunction formed by a donor and an acceptor. This architecture is necessary to enhance the spliting of the exciton into two charge carriers, which are then transported to the electrodes by the same materials which are used for the generation of the exciton. Consequently, materials for organic photovoltaic devices should be able to both harvest light and transport charge carriers efficiently, a difficult task to achieve.

The dye-sensitized solar cell (DSC) has key advantages over silicon based solar cells such as the low-cost of fabrication, low embodied energy cost, and the higher efficiency at low insolation level [1,2]. It also has important advantages over organic solar cells, as the generation of charge carriers and the transport of these charges are achieved by different materials [3,4].

DSCs are constructed from five key components: (1) a mechanical support coated with transparent conductive oxides (TCO); (2) a n-type semiconductor film of TiO_2; (3) a sensitizer chemically adsorbed onto the surface of the semiconductor; (4) an electrolyte containing a redox shuttle; (5) a counter electrode to regenerate the redox shuttle [4,5].

A schematic of the operating principles of the DSC is shown in Fig. 1. First, upon absorption of a photon, the sensitizer S is excited to S^*, which injects an electron into the conduction band of the

* Corresponding author. Tel.: +44 121 414 2527.
E-mail address: e.baranoff@bham.ac.uk (E. Baranoff).

http://dx.doi.org/10.1016/j.poly.2014.04.051
0277-5387/

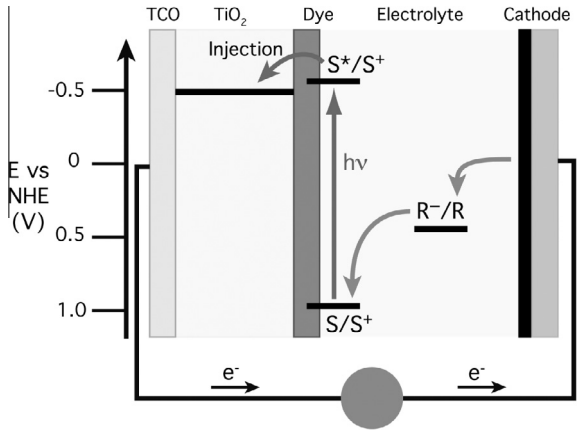

Fig. 1. Operating principles and energy level diagram of the DSC; $S/S^+/S^*$ = sensitizer in the ground, oxidized, and excited state; R^-/R = redox mediator.

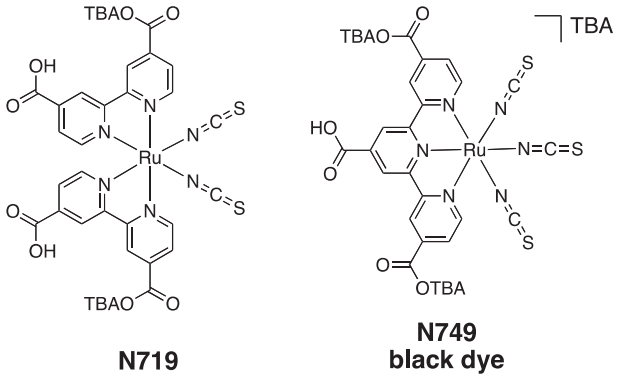

Fig. 2. Archetypal polypyridine ruthenium complexes for DSCs. TBA = tetrabutyl ammonium.

semiconductor. The resulting oxidized dye S^+ is regenerated by the redox mediator, which is in turn reduced at the cathode.

$$\eta = \frac{J_{ph} \cdot V_{OC} \cdot ff}{P_{irr}} \quad (1)$$

The power conversion efficiency (η) of the device is related to the photocurrent density (J_{ph}) also refered as short circuit current density (J_{sc}), the open circuit potential (V_{OC}), the fill factor (*ff*) of the cell, and the intensity of the incident light (P_{irr}), (Eq. (1)).

The sensitizer is a key component for high efficiency devices as it dictates the light harvesting capability of the device (related to J_{ph}) and participates in the electron transfer dynamics (related to V_{OC} and *ff*). Therefore optimization of the photophysical and electrochemical properties of the sensitizer has been the subject of intensive work.

Historically, polyimine ruthenium complexes have had a particular importance and were central to the early successes of the DSC [3,5], resulting in champion cells with 11% power conversion efficiency under AM1.5 conditions [6]. In particular since black dye was first reported, ruthenium complexes with tridentate ligands have attracted attention due to their ability to harvest photons in the near infrared. Herein we review this family of sensitizers for dye-sensitized solar cell focusing on their chemical structures and properties. We briefly highlight their performance in photovoltaic devices.

2. Archetype ruthenium dyes: N719 and N749

Several transition-metal complexes have been tested as sensitizers for DSCs [7–16]. Within this large family of sensitizers, the best photovoltaic performances both in terms of conversion yield and long term stability have so far been achieved with complexes of ruthenium in which polypyridine (substituted with carboxylic acid functional anchoring groups) and thiocyanate ligands have been used (see Fig. 2).

The ruthenium complex cis-$Ru(dcbp)_2(NCS)_2$, dcbp = 4,4′-dicarboxy-2,2′-bipyridine, known as **N3** dye, has become the paradigm for heterogeneous charge transfer sensitizers in dye-sensitized solar cells [17]. The doubly deprotonated version, **N719**, offers an improvement in the device performance due to the impact of the protons on the properties of the complex and on the conduction band of the titania. The role of the carboxylate groups is to anchor the sensitizer onto the surface of the semiconductor film via the formation of bidendate coordination and ester linkages. The thiocyanate groups stabilize the dye t_{2g} orbitals, finely tune the oxidation potential of the dye to match the potential of the iodide/triiodide redox mediator and also enhance the visible light absorption. Under AM 1.5 solar light, a DSC using **N719** exhibited 17.73 ± 0.5 mA current, 846 mV potential and a fill factor of 0.75 yielding an overall conversion efficiency of 11.18% [6].

N719 exhibits absorption maxima (extinction coefficient) at 395 nm ($1.43 \times 10^4\ M^{-1}\ cm^{-1}$) and 535 nm ($1.47 \times 10^4\ M^{-1}\ cm^{-1}$) due to metal-to-ligand charge transfer (MLCT) transitions involving the t_{2g} metal orbitals and the π^* orbital of the bipyridyl ligand [18]. The absorption depends on the pH of the solution and the absorption maxima are blue shifted upon deprotonation (Fig. 3a). Most importantly, in device conditions, the spectral response of **N719** barely exceeds 780 nm, while the optimum threshold for single junction converters is 920 nm.

N749, or black dye, was developed to absorb more of the visible spectrum. It uses a terpyridine ligand, 4,4′,4″-tricarboxy-2,2′:6′,2″-terpyridine (tctpy), and three –NCS. When going from $Ru(bpy)_3^{2+}$ (bpy = 2,2′-bipyridine) to $Ru(tpy)_2^{2+}$ (tpy = 2,2′:6′,2″-terpyridine), the absorption maximum is red shifted from 452 to 474 nm [19]. An even larger red shift of absorption is observed between **N719** (535 nm) and **N749** (610 nm) [20]. This effect is attributed to the modification of the polypyridyl ligands and to the additional –NCS group, which supplies a further negative charge to the metal center and destabilizes the HOMO energy level (E_{ox} = 0.85 and 0.66 V *versus* SCE for **N719** and **N749**, respectively), which in turn reduces the optical bandgap. The absorption spectrum of **N749** also depends on the pH of the solution and is blue-shifted upon deprotonation (Fig. 3b) [20]. A nanocrystalline photoelectrochemical cell sensitized by **N749** resulted in η = 10.4% with V_{OC} = 0.72 V, J_{ph} = 20.53 mA m^{-2} and *ff* = 0.704 [20]. Optimization of the device leads to a conversion efficiency slightly above 11% [21,22]. Despite the spectral response reaching 920 nm, which is the ideal value for single junction cells, the conversion efficiency improvement over **N719** is not as significant as one might expect. This is due to the lower driving force of dye regeneration by the electrolyte and a lower coupling with the TiO_2 density of states lowering the injection efficiency compared to **N719** [23,24].

3. $RuL(NCS)_3$ type of complex with L = tridentate ligand

The unique near infrared sensitization of titania by black dye triggered a lot of interest and engendered many studies on this particular sensitizer. Yet most chemical modifications of black dye have only recently been reported.

Complexes **1**–**3** (Fig. 4) utilize the same strategy of extending the conjugation of the terpyridine ligand to further increase the response in the near infrared [25,26]. The synthesis of the complexes follows a two-step procedure: the terpyridine ligand is first refluxed with ruthenium trichloride in ethanol to afford $RuLCl_3$,

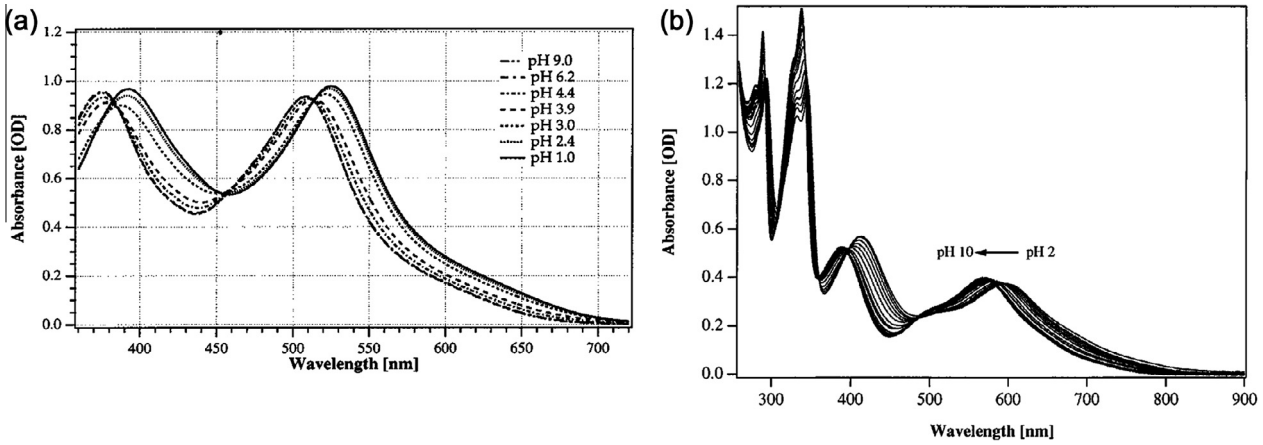

Fig. 3. Absorption spectra upon variation of pH of (a) **N719** (Adapted with permission from ref. [18]. Copyright 1999 American Chemical Society) and (b) **N749** (Adapted with permission from Ref. [20]. Copyright 2001 American Chemical Society).

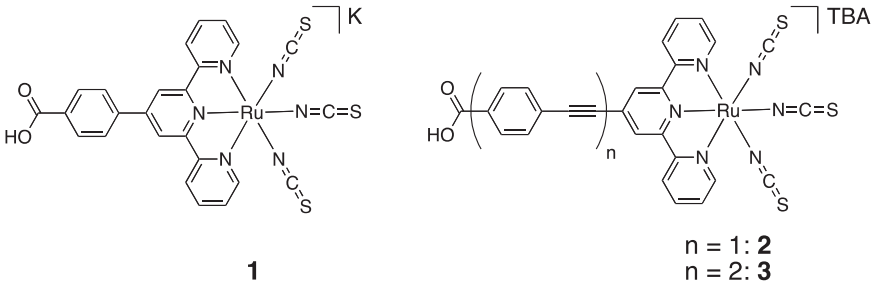

Fig. 4. Chemical structures of complexes **1**–**3**.

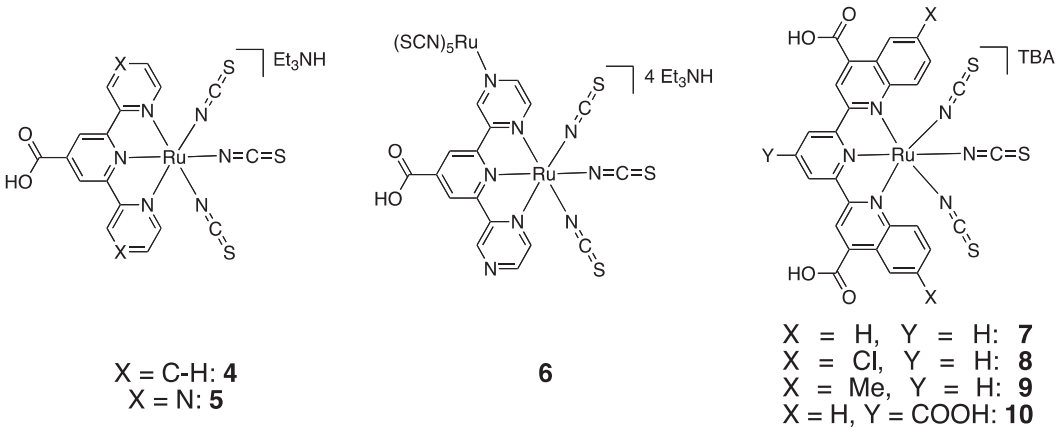

Fig. 5. Chemical structures of complexes **4**–**10**.

which is subsequently reacted with the thiocyanate salt in a mixture DMF/water. The lowest energy absorption peak of a solution of **1** in ethanol is at 560 nm and extends up to 800 nm. It is therefore blue shifted compared to **N749** due to the different number of carboxylic acid groups [25]. A device using **1** was made and compared to the same device using **N3** (the fully protonated version of **N719**). Despite the panchromatic response of **1** compared to **N3**, the device using **1** is only 2.9% efficient (for **N3**, efficiency is 6.8% at a light intensity of 78 mW cm^{-2}) due mainly to the large difference of photocurrent (6.1 and 14.5 mA cm^{-2} for **1** and **N3**, respectively).

The use of phenylene-ethylene units in **2** (1 unit) and **3** (2 units) counters the removal of carboxylic acids and **3** exhibits a low energy tail in absorption similar to **N749** with stronger absorption in the 450–600 nm region (1.2×10^4 M^{-1} cm^{-1} compared to 0.8×10^4 M^{-1} cm^{-1}) [27]. The oxidation potentials have been measured and both are at 0.56 V *versus* SCE which is 0.1 V less positive than **N749**. Complex **2** results in a better conversion efficiency compared to **3**, 5.7% and 2.4% respectively, which is attributed to a difference in how the complexes aggregate [26]. It could also be due to the increased distance between the ruthenium and the TiO_2 surface in **3**, which would lower the injection efficiency.

Another approach to modify the properties of black-dye-type complexes is to exchange a pyridine group with another heterocyclic moiety (see Fig. 5). Complex **4** was prepared as a model to complex **5** where two pyridines have been replaced by more

electron-withdrawing pyrazine rings [27]. In contrast to **1–3**, it was necessary to use the ester version of the ligand to prepare **4**. The attempt to synthesize **5** following the same method possibly resulted in the unexpected complex **6**. Although the structure is not demonstrated, it would correspond to the analytical characterization. Complex **6** presents a very broad absorption band extending further into the near infrared than **N749**, while **4** is slightly blue shifted to 588 nm. Devices using black dye outperform devices using **4** both in terms of photocurrent (10.23 *versus* 6.19 mA cm^{-2}) and open circuit voltage (717 *versus* 616 mV). Study of the electron dynamics indicates that more recombination occurs in devices with **4** [27].

The series of complexes **6–10** use two quinolines instead of two pyridines in the terdentate ligand to extend the light-harvesting properties of the sensitizer in the near infrared region [28,29]. The extended aromatic structure of the ligand increases the delocalization compared to the terpyridine and therefore lowers the energy of the π^* orbitals leading to absorption extended towards the lower energies.

The absorption spectrum of **7** is compared to black dye in Fig. 6. Hyperchromic absorption bands are observed in the UV region and a broad MLCT absorption band is present between 500 and 900 nm. Most remarkably this band extends about 100 nm more into the near infrared region than **N749**. However, the effect on the light harvesting performance is limited. The photocurrent action spectra (Fig. 6) shows that **N749** is much better at harvesting photons between 400 and 850 nm. Although **7** absorbs further into the infrared, the overall gain in photon absorption is small [28]. **N749** has an already limited injection efficiency due to its low LUMO energy level [23,24]. The quinolone moiety further lowers the LUMO energy level, and thus the power conversion efficiency is significantly restricted by the injection.

The introduction of chloride substituents in **8** results in a small red shift in absorption compared to **7**. However the photocurrent action spectrum and in turn the efficiency of devices using **8** are much lower than those sensitized by **7**. The chloride substituents act as acceptor groups further lowering the energy of the LUMO as demonstrated by theoretical calculations [29]. This confirms the impact of the injection on the performance of the devices. The replacements of chlorides with methyl groups in **9**, which have some electron donating character, improve the efficiency, but not as much as **7** [30]. Complex **10** has an additional anchoring group, which acts as an acceptor group, but also improves the contact of the dye with the titania. These two antagonistic effects cancel each other out and overall the same power conversion efficiency as **9** is obtained [30].

Theoretical calculations [23,31,32] and vibrational spectroscopic studies [33] indicate that adsorption of black dye onto titania occurs *via* only two carboxylic groups. This research has given rise to a range of dyes in which one anchoring group is replaced with a thiophene-based substituent in an attempt to improve the absorption properties of the sensitizer (see Fig. 7) [34]. Complexes **11**–**14** were prepared from the reaction of the ester-version of the terpyridine ligands with ruthenium trichloride, followed by exchange of the chlorides with –NCS, and finally hydrolysis of the ester groups. All four dyes have similar redox potentials (E_{OX} = 0.84 to 0.89 V *versus* NHE and E_{RED} = –0.77 to –0.85 V *versus* NHE) as well as similar emission maxima (λ_{em} = 813 to 820 nm).

The absorption spectra of dyes **11**–**14** in methanol solution are compared to **N749** in Fig. 8. All dyes have an absorption band assigned to a MLCT transition from the metal center to the terpyridine at about 600 nm, slightly blue-shifted compared to **N749** [34]. Only **14** displays an intensity higher than **N749** for this MLCT band. The overall lower absorption of these complexes is attributed to the absence of the third carboxyl group. A major effect of the substituents is found between 350 and 500 nm. Increasing the electron donating capability and elongating the π conjugation of the substituent from **11** to **14** results in an intense absorption band (Fig. 8). This effect can also be observed in the photoaction spectra of the devices (Fig. 8) as an increased IPCE (incident photon conversion efficiency) value at higher energies. Remarkably, all the substituted complexes **12–14** give a higher photocurrent than devices using **N749**; moreover the device using **13** as the sensitizer has a power conversion efficiency of 10.3% compared to 8.54% for the same device using **N749** [34].

To gain understanding of the reasons behind such result, a study of the carrier dynamics of these devices was done [35]. Among other reasons (including the increased light harvesting abilities) it was found that **13** exhibits an improved injection efficiency compared to that of **N749**.

A series of complexes with a similar design to **12** was recently reported (Fig. 9) [36]. **15**–**17** contain phenyl and thiophene moieties substituted with hexyl chains. As expected, the features in absorption for **15**–**17** are similar to **12** and the oxidation potentials are also comparable (E_{OX} = 0.87 to 0.86 V *versus* NHE). The reduction potentials are also in the same range reported for **11**–**14** (E_{RED} = −0.76 to −0.82 V *versus* NHE). It was found that **16** gives the best efficiencies, close to the value obtained with **N749** (8.7% compared to 9.2%). **16** was used as a basis for further modification, through the addition of bulky dihexyloxyphenyl groups, complexes **18–20**. The rationale stems from the results obtained with organic dyes, in which it was found that bulky substituents limit the

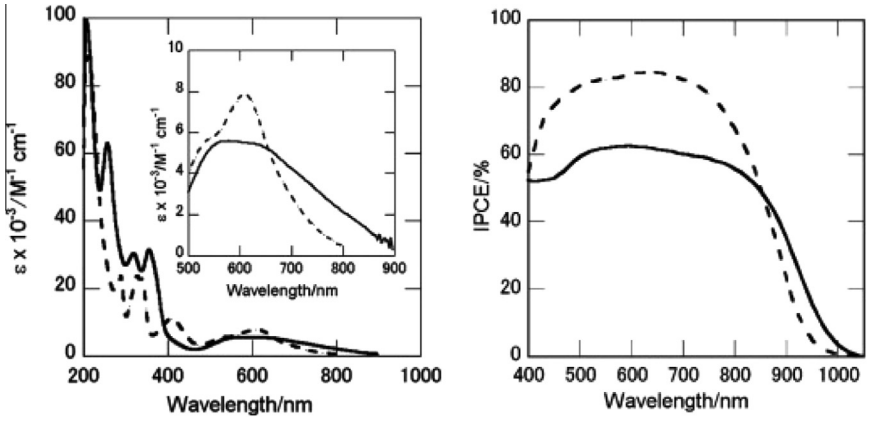

Fig. 6. Left: absorption spectra of **7** (solid line) in methanol and black dye (dashed line) in ethanol. Right: Photocurrent action spectra for DSCs sensitized with **7** (solid line) and with black dye (dashed line). From ref. [28].

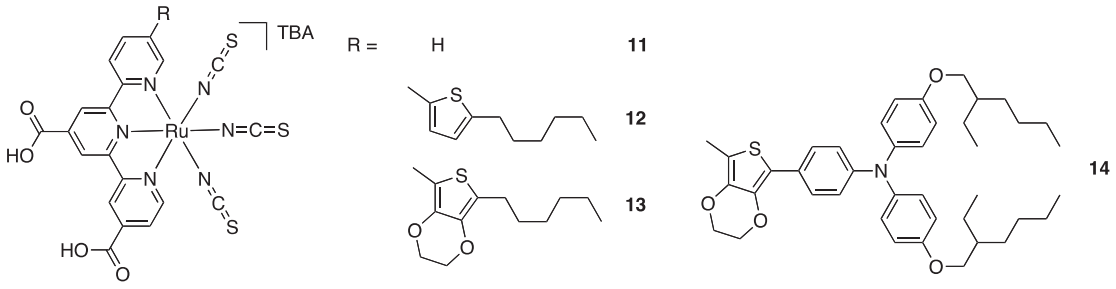

Fig. 7. Chemical structures of complexes **11**–**14**.

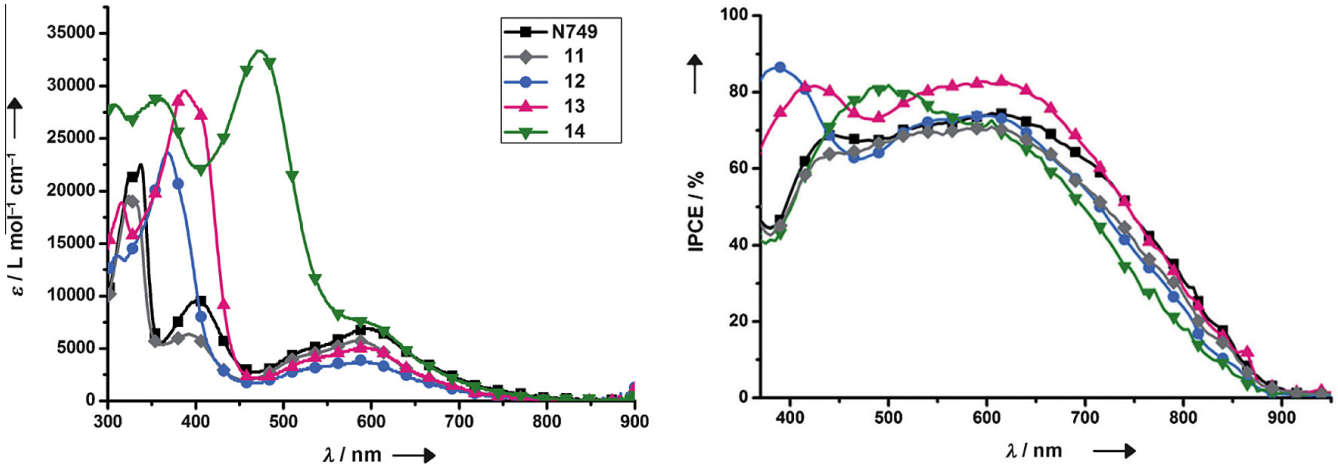

Fig. 8. Left: absorption spectra of N749 and sensitizers **11**–**14** recorded in methanol. Right: IPCE spectra of the 15 + 5 mm devices. From Ref. [34].

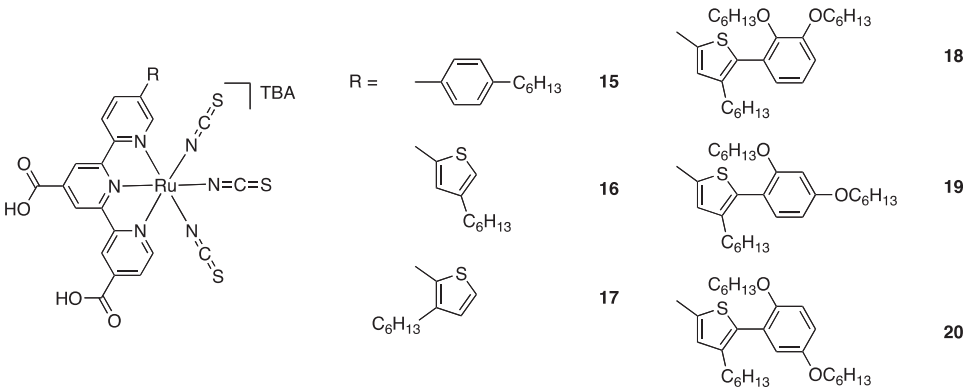

Fig. 9. Chemical structures of complexes **15**–**20**.

recombination of electrons from the TiO_2 directly with the redox mediator. The absorption maximum of the low energy MLCT band is red shifted to 630 nm and the oxidation potential drops to 0.82 V *versus* NHE for the three complexes [36]. This reflects the increased electron donating character of the new substituents. Virtually identical power conversion efficiencies are found for **19** and **N749** (9.1% and 9.2%) using iodide/triiodide as the redox mediator. Initial results using $Co(bpy)_3^{2+/3+}$ as the redox mediator results in better performance with **19** than with **N749** (2.2% and 0.6%).

A series of substitutions at the 4 position of one of the flanking pyridine has been carried out in another investigation of modifications to the black-dye archetype (see Fig. 10). In complex **22**, the conjugation has been extended with a methylstyryl group [37]. In methanol, **22** shows panchromatic absorption with higher absorption intensity than **N749** over the entire spectrum, in

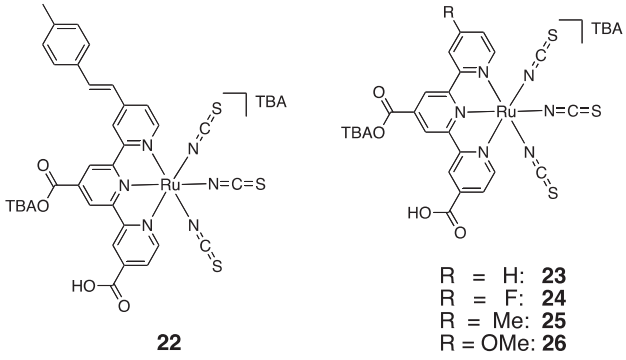

Fig. 10. Chemical structures of complexes **22**–**26**.

particular a shoulder at 685 nm, which is of interest for harvesting low energy photons. In addition the LUMO of **22** lies at a higher energy than of **N749**. These attractive features in solution are translated into device efficiency and a DSC constructed with **22** has a higher efficiency (11.1%) than the same device made with **N749** (10.5%). This improved performance is due to a higher photocurrent (23.07 mA cm^{-2} compared to 21.28 mA cm^{-2}) [37].

This interesting result was labeled "serendipitous" by the authors and they engaged in a systematic study of the substituted complexes **23**–**26** to gain understanding of the influence of the electron-donating and -withdrawing groups on the properties and performance of this system [38]. It was found that fluorine leads to an increased charge recombination and decreased electron injection efficiency, while a methyl group leads to the best results.

4. RuLL'(NCS) type of complex with L = tridentate ligand, L′ = bidentate ligand

Two disadvantages of the –NCS ligand are its ambidenticity, leading to possible linkage isomerism, and its monodenticity, possibly resulting in loss of the ligand. To overcome these, bidentate ligands have been explored to replace two –NCS ligands in order to improve the stability of the sensitizer.

The first type of bidentate ligands to be used in combination with a tridentate ligand for ruthenium complexes are derivatives of 1,1,1-trifluoropentane-2,4-dionato (complex **27** in Fig. 11). Complex **28** possesses a long alkyl chain to suppress dye aggregation on the TiO_2 surface [39]. The complexes were synthesized by first refluxing Ru(4,4′,4″-trimethoxycarbonyl-2,2′:6′,2″-terpyridine)Cl_3 in methanol in presence of the dione derivative with triethylamine as a base, followed by reaction with NaSCN. Finally the esters are hydrolysed with triethylamine and the crude products purified with Sephadex LH-20 to give the complexes in approximately 50% yield.

Both complexes exhibit virtually the same absorption spectra. The absorption bands in the UV region are assigned to intra ligand π–π^* transitions of the terpyridine ligand, as with other ruthenium complexes. A broad and intense (ε = 7000 M^{-1} cm^{-1}) MLCT band at 610 nm is the main feature in the visible region of the spectrum with a shoulder at 720 nm. Due to this shoulder, the absorption above 700 nm is significantly enhanced in **27** and **28** compared to that of **N749** [39]. Broad luminescence above 900 nm is observed in degassed solutions. The oxidation potentials have been measured for the complexes in solution in methanol and are 0.70 and 0.78 V *versus* SCE for **27** and **28**, respectively.

With deoxycholic acid as an additive to limit aggregation, the IPCE spectra of **27** and black dye are shown in Fig. 12. Importantly, **27** displays a higher IPCE in the 720–900 nm region. Complex **28** does not require the co-adsorbant to reach a high IPCE, demonstrating the effectiveness of the long alkyl chain at limiting dye aggregation [39].

In the series of complexes **29–31** that include a phenyl group on the dione ligand, the absorption is blue shifted by about 20 nm compared to **27** [40]. Nevertheless, improved power conversion efficiencies are observed possibly due to the more positive oxidation potential (~0.73 V *versus* SCE compared to 0.68 V *versus* SCE for **27**) which favours regeneration of the dye. A device made using **30** as the sensitizer reaches a power conversion efficiency of 9.1%.

To further improve the light harvesting ability of this type of complex and tune the energy level of the HOMO for efficient dye regeneration, complex **32** was prepared with an appended diphenylamino group. Comparison was then made with **27** [41]. The absorption coefficient of **32** is 40% higher than **27** over the entire spectrum. In addition a distinct shoulder at around 700 nm further enhances the absorption in the near-IR region. This results in an increased light-harvesting efficiency in the near infrared giving a higher photocurrent of 19 mA cm^{-2}.

A complex with a 2-quinolinecarboxylate ligand in place of the acetylacetonate derivatives was also reported [42]. It shows improved absorption between 400 and 450 nm compared to black dye and possesses an additional shoulder at 700 nm. While the photocurrent generated is similar to the one generated by black dye, the *ff* and V_{OC} are slightly lower resulting in a lower efficiency (8.1% compared to 8.8% for the black dye).

Cyclometalated 2-phenylpyridine (ppy) ligands have been used in place of the acetylacetonate derivatives. Complex **33**, Fig. 13, was prepared as a model for complex **34**, which has a phenyl-ethynyl group to improve the absorption properties of the sensitizer [43]. The cyclometalation was achieved with triethylamine in a mixture of ethanol and water. The HOMO is delocalized over the –NCS, the ruthenium and the orthometallated phenyl group while the LUMO remains mainly on the terpyridine ligand.

The absorption spectra of **33** and **34** in basic methanol are shown in Fig. 14. Interestingly, the cyclometalated complexes display absorption bands around 740 and 800 nm with the tail extending up to 900 nm. These bands have been attributed to spin-forbidden MLCT transitions [44]. The molar extinction coefficient of **34** was higher than that of **33** over the entire spectrum because of the extension of the π-system. The photocurrent action spectra of DSCs using **33** and **34** extend up to 1000 nm. However the photocurrent generated is low, possibly due to the low driving force for regeneration [45].

To tune the HOMO energy level, ppy has been replaced by 2-phenylpyrimidinato (ppym) moieties, and trifluoromethyl groups have been added on the orthometallated phenyl part (complexes **35**–**37**) [45]. The absorption spectrum of **35** extends up to

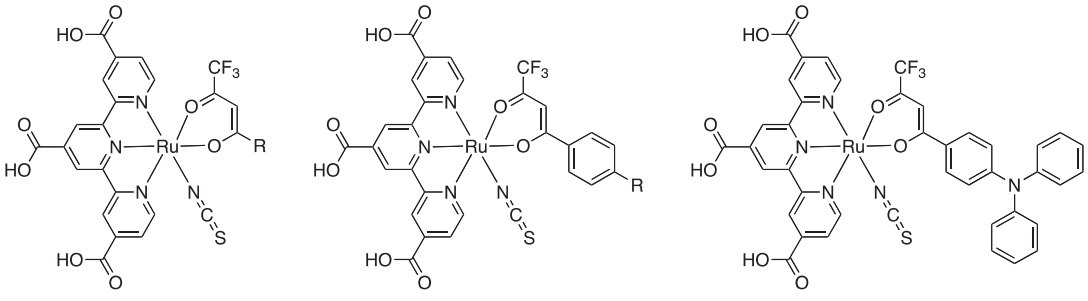

Fig. 11. Chemical structures of complexes **27**–**32**.

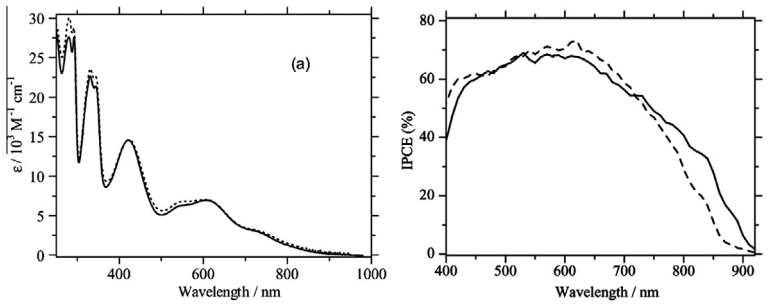

Fig. 12. Left: absorption spectra of **27** and **28** in ethanol-methanol (4:1 v/v). Right: photocurrent action spectra of **27** (–) and black dye (—). From Ref. [39].

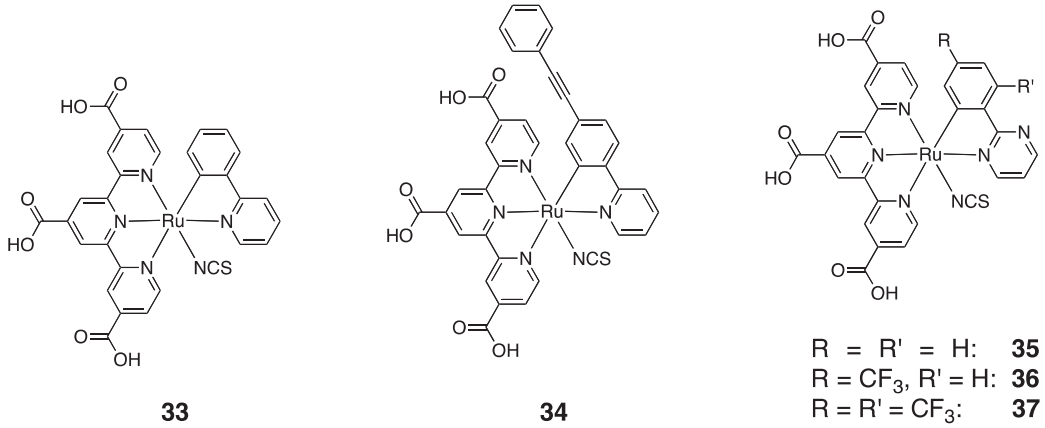

Fig. 13. Chemical structures of complexes **33**–**37**.

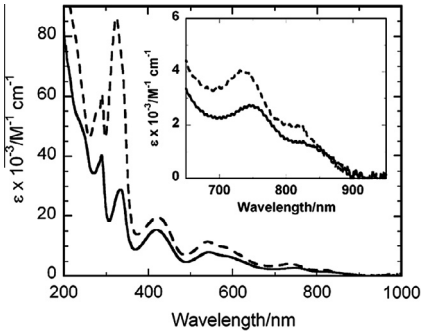

Fig. 14. Absorption spectra of **33** (solid line) and **34** (dashed line), measured in 1×10^{-3} M TBAOH methanol solution. From Ref. [43].

1000 nm and the introduction of $-CF_3$ groups blue shifts the absorption. Nevertheless, all complexes absorb more in the red than **N749**. The additional effect of $-CF_3$ is to stabilize the oxidation potential: E_{OX} = 0.49, 0.52 V *versus* SCE for **36**, and **37**, respectively, compared to 0.42 V for **35** [45]. Although **37** is the least red absorbing complex in the series, it results in DSC with higher power conversion efficiency than devices using **N749**, 10.7% compared to 10.1%, due mainly to an increased photocurrent compared to **N749**.

Another approach to a monoanionic bidentate ligand is to use a pyridine pyrazolate where the –NH of the pyrazole is deprotonated [46]. The heteroleptic complexes **38**–**41** (Fig. 15) display significantly higher molar extinction coefficients at 400–550 nm compared to black dye. In addition the absorption onset extends well into the longer wavelength region >800 nm. The pyrazolate ligand is less electron donating than the two thiocyanate ligands it replaces and it is also a less effective donor than ppy-type ligands. Consequently the absorption maximum of the main MLCT band is centered at 520 nm, significantly blue shifted compared to **N749** and **33**–**37**. Nevertheless, the performance of these complexes in DSCs has been found to be superior to devices with black dye as the sensitizer. In the series, **41** performs best with a power conversion efficiency just above 10% compared to just above 9% for black dye [46]. This is due to an improvement in both V_{OC} and photocurrent. The stability of a DSC using **41** as the sensitizer has been studied under AM 1.5G irradiance at 60 °C. After 1000 hours illumination, the efficiency drops from 4.46% to 4.06% [46]. The different initial efficiency compared to high-efficiency cells is due to a change of architecture (7 μm transparent TiO_2 thin film instead of 18 μm) and a switch to nonvolatile electrolyte. In a modification where the anchoring ligand is a dicarboxybipyridine and the pyrazolate is on the tridentate ligand, the performance of the DSC approaches that of the device using **N3** [47].

With complexes **42** and **43**, a new class of cyclometalated ruthenium sensitizers was reported. The anionic charge does not originate from the bidentate ligand, which is a neutral bipyridine derivative, but from the tridentate ligand as the terpyridine is replaced by a cyclometalating phenyl-bipyridine [48]. The synthesis of the complexes followed a different strategy from previous complexes containing a terpyridine ligand. The bis-thiophenylbipyridine was reacted first with the dichloro(*p*-cymene) ruthenium(II) dimer in DMF at 80 °C for 4 h. Then the phenylbipyridine was added and the mixture stirred at 160 °C for 4 h. Finally NH_4NCS was added and the solution heated 8 h at 140 °C. Standard purification gave a pure complex in 60% (**42**) and 45% (**43**) yield.

The UV–Vis electronic absorption spectra of **42** and **43** in EtOH exhibit a MLCT transition at 527 and 530 nm, respectively [48]. The red-shifted absorption observed in **43** is attributed to the more electron rich π-conjugation unit in an ancillary ligand. The molar extinction coefficients of these two peaks are above

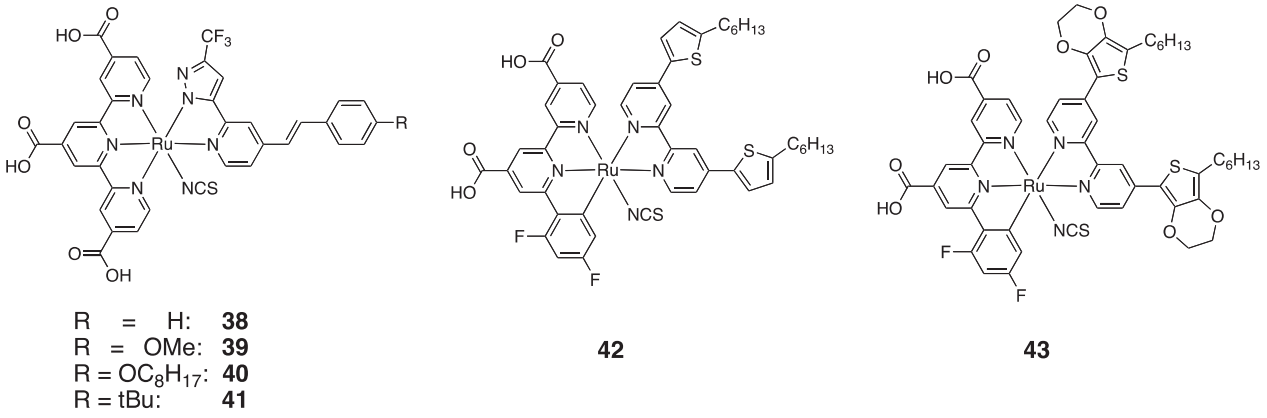

Fig. 15. Chemical structures of complexes **38**–**43**.

15 000 M^{-1} cm^{-1}, which is more intense than the aforementioned RuLL'(NCS) sensitizers. However, the absorption extends just above 750 nm and the properties are compared to **N719**. Despite this a power conversion efficiency of 10.4% has been obtained with **42**; the performance drops to 6.3% conversion efficiency with **43** due to a significant decrease of the photocurrent. The stability of a DSC device using **42** as the sensitizer was found to be improved compared to the same device using **N719**, under AM 1.5G irradiation and at 60 °C. After 1000 hours irradiation, the efficiency drops from 7.14% to 6.51% while the decrease of efficiency is from 7.03% to 5.25% with **N719** [48].

It should be noted that ruthenium complexes RuLL'(NCS), L = 4,4′,4″-tricarboxylate-2,2′:6′,2″-terpyridine (tctpy) and L' = 4,4'-R-2,2'-bipyridine with R = vinyl substituents, have been reported [49,50]. However the absorption properties are significantly limited with the main MLCT band below 500 nm and extension of the absorption only slightly above 700 nm. This demonstrates the importance of the anionic character of the ancillary ligand (e.g. pyrazolate, cyclometalated) to achieve panchromatic absorption extending into the near infrared.

5. RuLL′ type of complex with L = tridentate ligand, L′ = tridentate ligand

The promising stability of complexes with only one –NCS combined with the possibility to easily modify the structure of the sensitizer and tune its photophysical properties prompted research into ruthenium complexes with two tridentate ligands. As such there are no ambidentate/monodentate –NCS groups coordinated to the ruthenium center.

The first bis-tridentate ruthenium complex for DSC application, **44** Fig. 16, was reported in 2007 [51]. It is a simple ruthenium(II) bis-terpyridine complex with one pendant carboxylic acid as the anchoring group. It displays an intense (ε = 18 000 M^{-1} cm^{-1}) and sharp MLCT band at 487 nm, which extends to about 640 nm only. As the result the IPCE of a DSC with **44** is poor. The addition of a thiophenyl group in **45** mainly results in a hyperchromic change of the MLCT band with ε = 24 000 M^{-1} cm^{-1} [52]. A similar hyperchromic change was observed when a second carboxylic acid was added in complex **46** [53]. The use of pyrazine in place of pyridine, **47**, is detrimental to the absorption properties of the complex as blue shifted MLCT band with lower intensity is observed [53].

A series of NHC carbene-based complexes, **48**–**49** Fig. 17, was tested as sensitizer for DSC [54]. The strong electron donating character of NHC carbene destabilizes the HOMO energy level of the complex, which is in turned stabilized due to the electron withdrawing character of the carboxylic acid. Incidentally, the replacement of two pyridine rings with two NHC carbenes is exactly offset by the addition of a second anchoring group in **50** compared to **48**–**49**. Consequently, the three complexes have the same oxidation potential, E_{OX} = 1.79 *versus* NHE [54]. However the use of a NHC carbene ligand results in a high lying LUMO, an effect only partially countered by the carboxylic acid group. As a result, the absorption of **50** is blue-shifted by 20 to 30 nm compared to **48**–**49** [54]. Despite the apparently unfavorable properties of **50**, the power conversion efficiency of DSC using **50** is 4 to 5 times higher than devices using **48**–**49**. Nevertheless, the device using **N719** has a much higher efficiency [54].

Introduction of benzimidazole groups in **51** mainly results in a suitable oxidation potential of 0.87 V *versus* NHE, the same as the black dye [55]. While the absorption properties of **51** are not significantly different from **44**, for example, with the MLCT band around 500 nm, the power conversion efficiency is promisingly close to a device using **N719** as the sensitizer, 6.05% and 6.47%, respectively [55].

As seen in section 4, cyclometalated ligands are an attractive way to improve the absorption of ruthenium sensitizers and this strategy has also been used for bis-tridentate complexes (see Figs. 18 and 19). The first cyclometalated ruthenium complex with

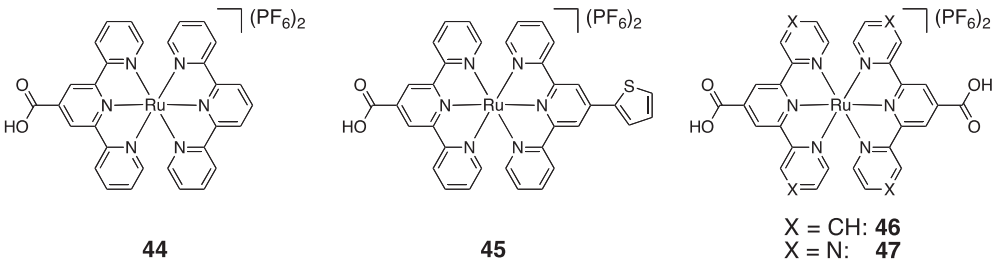

Fig. 16. Chemical structures of complexes **44**–**47**.

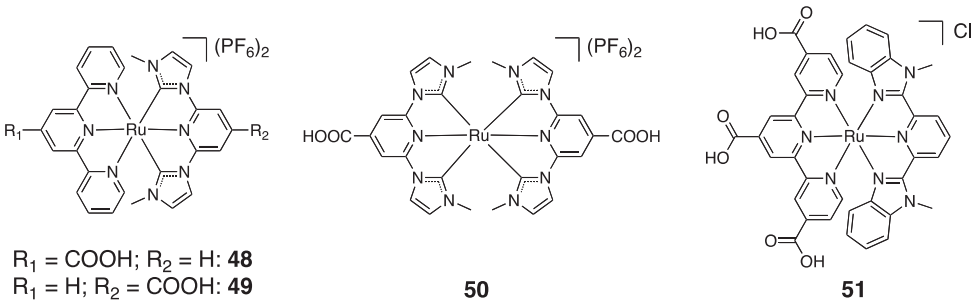

Fig. 17. Chemical structures of complexes **48**–**51**.

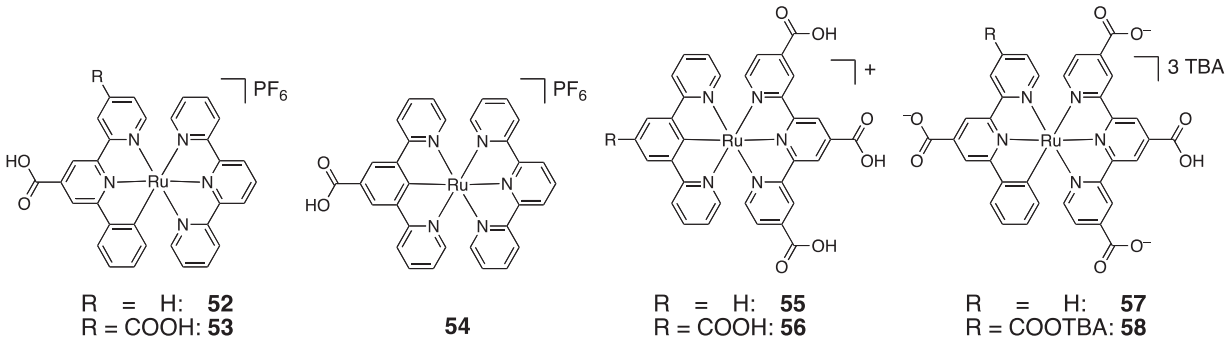

Fig. 18. Chemical structures of complexes **52**–**58**.

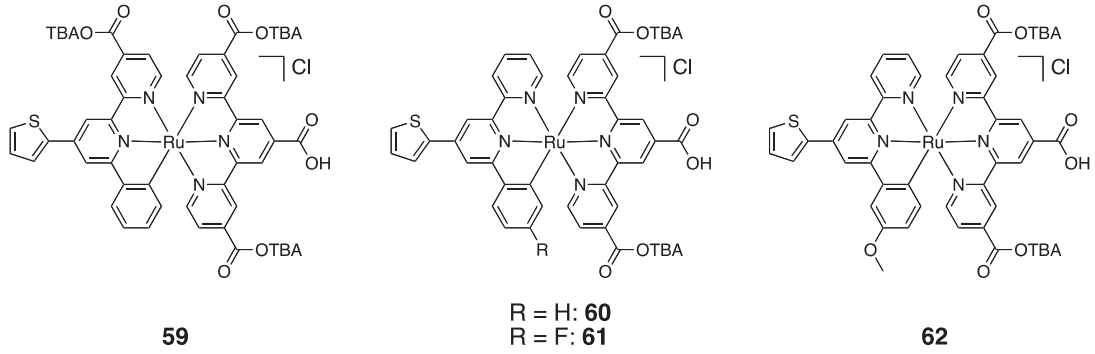

Fig. 19. Chemical structures of complexes **59**–**62**.

two tridentate ligands are **52**–**53** [51]. Compared to the non cyclometalated analogue **44**, the MLCT absorption band of **52** is red shifted by 36 nm and tails above 700 nm. As such **52** has an absorption spectrum similar to **N719** except for around 400 nm where its absorption is less intense. The addition of a second carboxylic acid in **53** further red shifts the absorption to 552 nm. Overall, DSCs with **53** and **N719** have quasi identical photocurrent action spectra [51]. Changing the position of the cyclometalated carbon in **54** has a significant impact on the absorption properties compared to **52** [56]. The absorption maximum of the MLCT transition is located at 492 nm with shoulders at lower energies. The net result is more intense absorption between 400 and 500 nm and reduced intensity above 500 nm for **54** compared to **52**. This blue shift of absorption is paralleled by an increase of the redox gap from 2.03 to 2.16. This increase of the redox gap is mainly due to a destabilization of the LUMO energy level in **54** compared to **52**, as seen in the first reduction potentials of −1.91 and −1.81 *versus* ferrocene/ferrocenium for **54** and **52**, respectively [56]. However, striking differences are observed when the IPCEs are compared as **54** gives an IPCE of less than 10% while **52** reaches 50%. This result was attributed to poor injection efficiency due to the excited state being localized on the terpyridine that is away from the TiO_2 surface in contrast to **52** where the excited state is located on the phenyl-bipyridine attached to the TiO_2 surface [56].

The effect of additional carboxylic acid groups, in particular with tctpy in complexes **55–58**, is to impart a second MLCT absorption band around 400 nm, similar to **N719** [57,58]. The HOMO is located on the cyclometalated ligand, which is away from the TiO_2, and the excited state is located on the tctpy. DSCs exhibit fair to good light harvesting efficiency over the entire visible spectrum. Interestingly, the IPCE of **55** extends above 900 nm, while the IPCE of **57** barely reaches 800 nm, pointing to a key effect of the position of the cyclometalated group [57,58].

The introduction of a thiophenyl group is a known strategy to obtain dyes with red shifted absorption and increased absorption coefficients. Dye **59** can be compared to dye **58** where a carboxylic acid has been replaced by thiophene. The maximum abosrption is slightly red shifted from 522 to 530 with increased aborption

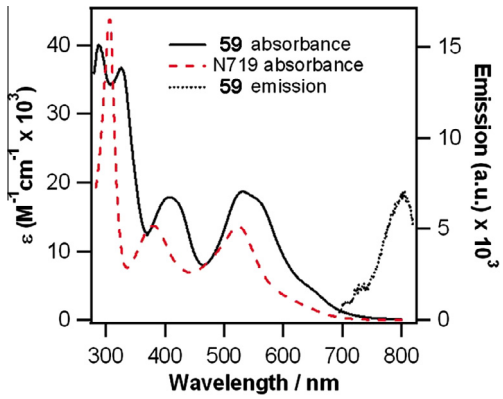

Fig. 20. Absorption (solid-black) and emission (dotted-black) spectra of **59** and absorption spectrum of **N719** in ethanol (dashed-red). From Ref. [59]. (Color online.)

intensity (16 000 M^{-1} cm^{-1} to 18 600 M^{-1} cm^{-1}). The shoulders of that band are also red shifted, in particular the lowest energy shoulder from 660 to 682 nm [59].

As a result, the absorption spectrum of **59** is red shifted with more intense absorption over the entire spectrum than **N719** (Fig. 20) [59]. Yet, the power conversion efficiency of a DSC using **59** as the sensitizer is below that of a device with **N719** due to a lower photocurrent. This was attributed to the difference in oxidation potential, 0.65 V *versus* NHE for **59** compared to 1.13 V *versus* NHE for **N719**, which would affect the efficiency of the regeneration of the oxidized dye by the redox mediator iodide/triiodide. The addition of CuI to the electrolyte resulted in a net increase of photocurrent to levels close to the one obtained with **N719** [59].

The complexes **60–62** were prepared to tune the redox potential of the ruthenium complexes [57]. The fluoride of **61** acts as an electron withdrawing group, increasing the oxidation potential from 0.90 V *versus* NHE for the non substituted complex **60** to 0.96 V *versus* NHE; the methoxy group acts as an electron donor, decreasing the oxidation potential to 0.87 V *versus* NHE. DSCs made with the three complexes have very similar photocurrents ~8.8 mA cm^{-2}. The V_{OC} increases with the redox potential. As a result, **61** provides the best power conversion efficiency of 3.06%, which is also helped by a slightly improved *ff* [57].

A series of cyclometalated Ru(II) complexes containing a thiophenyl and a triphenylamine (TPA) group, **63–66** (Fig. 21), were reported [60]. TPA substituents are attractive as they produce intense absorption bands in the visible region arising from multiple MLCT and ILCT (intraligand charge-transfer) transitions. In complexes **63–66**, different substituents are used on the TPA unit. The impact on the electronic absorption spectra is negligible and intense absorption bands are observed at ~435 and 526 nm for all complexes. While the Ru(III)/(II) is not affected by the remote substituents (1.17 V *versus* NHE), the oxidation potential of the TPA unit decreases as more donor substituents are used. Remarkably it is more positive than the ruthenium oxidation for **63** (1.22 V *versus* NHE), but is less positive for **64** (1.11 V *versus* NHE) and **65** (0.99 V *versus* NHE), which facilitates the interaction with the electrolyte. As a result, complex **65** gives the best power conversion efficiency (8.02%) [60].

Complex **66** offers insights into the impact of the position of the cylcometalated unit when compared to **64**. The visible light absorption is reduced both in terms of panchromaticity and intensity of absorption, as observed with **52** and **54**, and the efficiency of the DSC is lower (3.90% compared to 6.33% for **64**) due to reduced photocurrent and V_{OC} [60].

With the success of complexes **38–41** with an anionic pyrazole as a N-coordinating ring, a series of complexes with an analogue terdentate ligand was reported, **67–70** Fig. 22 [61].

The absorption spectra of **67–70** are compared to **N749** in Fig. 23. Besides the non substituted complex **67**, which shows similar absorption intensity to **N749**, the complexes display visible absorption bands between 370 and 560 nm with intensity up to three times that of **N749**. The bands are assigned to MLCT transitions from the ruthenium center to tctpy with some contributions from ligand-to-ligand charge transfer (LLCT) originating from the pyrazolate groups. In addition, all the dyes exhibit a broad absorption above 600 nm with a shoulder extending to 800 nm. The oxidation potentials of the dyes are about 0.95 V *versus* NHE [61].

The photocurrent action spectra are shown in Fig. 23. The onsets of the spectra are all close to 820 nm, about 100 nm below that of a DSC using **N749**. Between 400 and 550 nm and at around 700 nm, all the complexes (excluding **67**) exhibit a significantly higher performance than N749, although at 600 nm and at energies lower than 750 nm black dye is more efficient. As a result, DSCs using **68–70** as the sensitizer show higher photocurrent, above 20 mA cm^{-2}, and better V_{OC} than DSC with **N749**, despite the better light harvesting ability of the black dye above 785 nm. Best results are obtained with **69** which leads to a device with a power conversion efficiency of 10.7% compared to 9.22% for **N749** [61]. These performances are a significant improvement over a homoleptic complex RuL_2 with L_2 = 5-(4′-carboxy-2,2′-bipyridin-6-yl)-3-(trifluoromethyl)-3-pyrazolate [47].

The concept was further explored with an array of different tridentate ligands. In the first series, complexes **71–74** Fig. 24, the

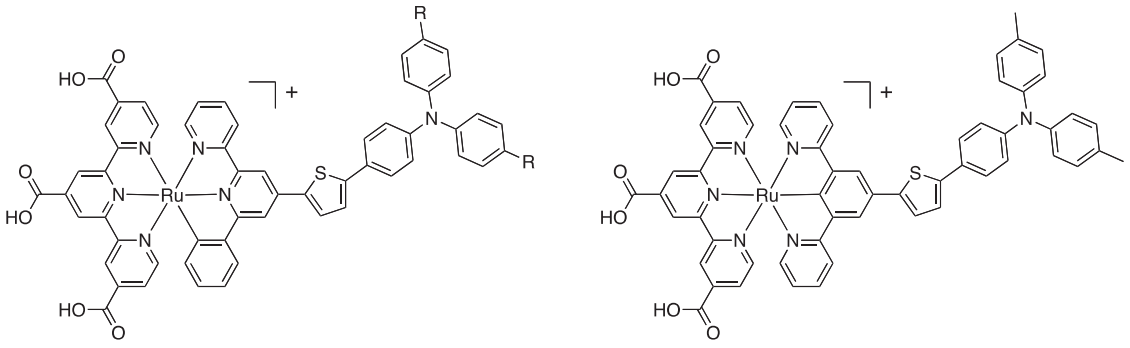

Fig. 21. Chemical structures of complexes **63–66**.

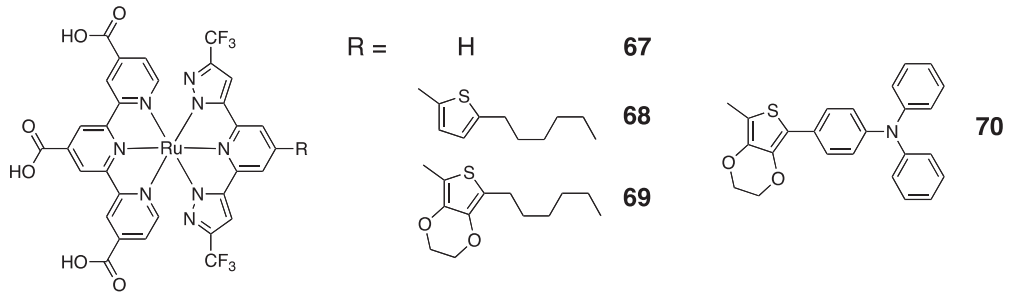

Fig. 22. Chemical structures of complexes **67**–**70**.

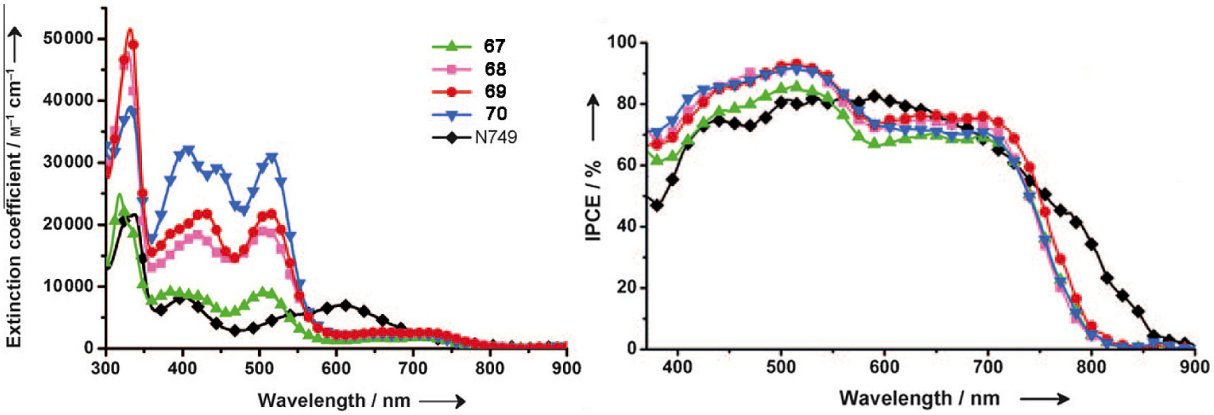

Fig. 23. Left: Absorption spectra of **67**–**70** and **N749** in DMF; Right: Photocurrent action spectra of solar cells sensitized with **67**–**70** and **N749**. From Ref. [61].

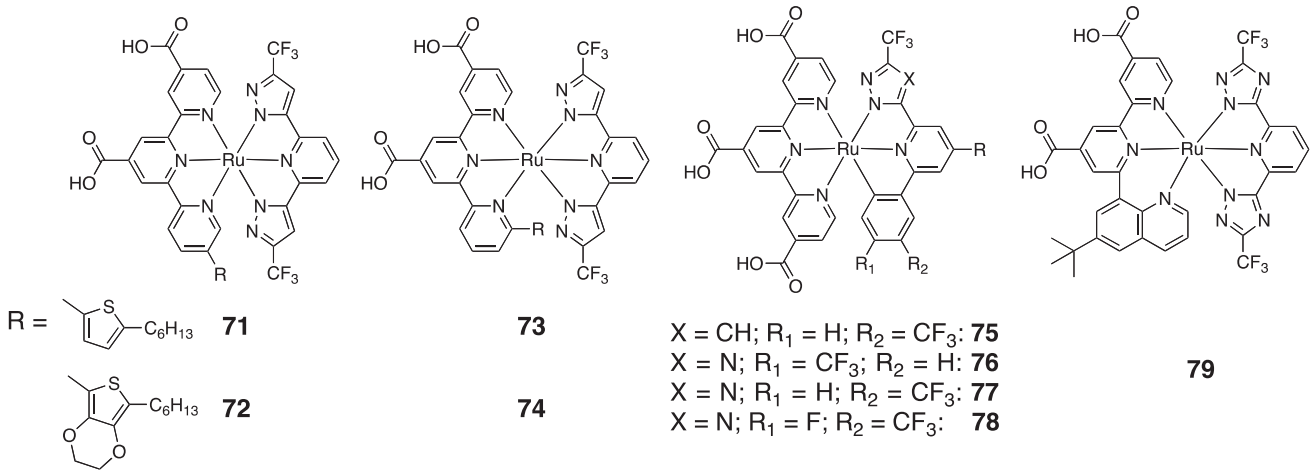

Fig. 24. Chemical structures of complexes **71**–**79**.

carboxylic acid of one of the flanking pyridines was removed and the pyridine substituted with hexylthiophenyl and hexyl-EDOT at the 5″ or 6″ position [62]. The complexes exhibit absorption bands centered at 510 nm, which is blue shifted compared to **N749** (600 nm). These bands are assigned to a MLCT transition to the dicarboxy-terpyridine ligand. **71** and **72** show an additional band at 363 and 389 nm, respectively. These bands are assigned to the intraligand π–π^* transition involving the thiophene and the EDOT pendant groups. In the case of **73** and **74**, these pendant groups may be orthogonal to the terpyridine chelate because of the steric hindrance from the 2,6-bis(5-pyrazolyl)pyridine chelate. Finally, **71–74** have broad absorption at longer wavelengths extending to 800 nm and assigned to spin-forbidden 3MLCT transitions [62].

In the second series, complexes **75–78** Fig. 24, one pyrazolate is replaced by an orthometalated phenyl group, **75**, and the second pyrazolate is also replaced with a 1,2,4-triazolate ring, **76–78** [63]. The replacement of a nitrogen donor by a formal carbanion donor would destabilize the oxidation potential of the complex due to a substantial increase of the electron density around the metal center. To counter this effect strong electron withdrawing groups have been grafted onto the orthometallated phenyl ring. The oxidation potentials are indeed close to that of **N749**, with **78** being the most positive due to the additional fluoride substituent. With regards to the UV–Vis absorption spectra, **75–78** display a stronger absorption than **N749** between 350 and 570 nm and a similar low energy tail [63].

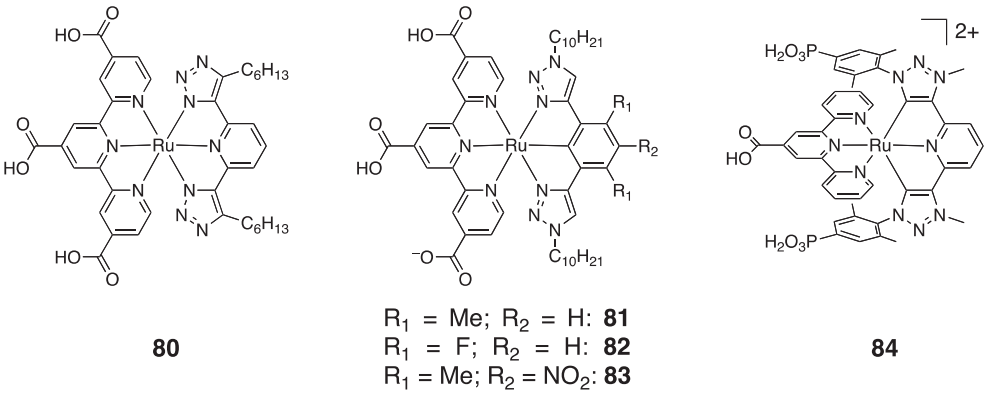

Fig. 25. Chemical structures of complexes **80–84**.

Table 1
Properties and device performance of key complexes.

	Code	λ_{abs} (nm) (e (10^3 M^{-1} cm^{-1}))	E_{OX} (V)[a]	E_{LUMO} (V)	J_{ph} (mA cm^{-2})	V_{OC} (V)	*ff*	η (%)	Ref.
42	JK-206	391 (19.8), 527 (18.0)	0.99	−1.00	19.63	0.74	0.72	10.4	[48]
68	TF-2	329 (47.9), 421 (18.4), 509 (19.2), 654 (2.5), 719 (2.4)	0.95	−0.73	20.00	0.79	0.67	10.5	[61]
69	TF-3	322 (51.6), 387 (18.8), 426 (21.9), 513 (21.9), 653 (2.7), 723 (2.6)	0.97	−0.75	21.39	0.76	0.66	10.7	[61]
70	TF-4	333 (39.0), 404(32.4), 447 (29.3), 516 (30.9), 662 (2.3), 716 (2.3)	0.94	−0.75	20.27	0.77	0.67	10.5	[61]
75	TF-21	324 (32.0), 404 (15.0), 520 (13.0), 703 (2.2)	0.84	−0.73	18.09	0.71	0.68	8.76	[63]
77	TF-23	313 (25.0), 329 (21.0), 402 (14.0), 517 (12.0), 693 (1.9)	0.92	−0.72	17.62	0.75	0.68	9.04	[63]
79	TF-32	404 (15.0), 519 (10.0), 647 (4.5)	0.82	−0.90	19.2	0.74	0.72	10.2	[64]

[a] Potentials given *vs* NHE.

Overall, most of these dyes give slightly higher photocurrents than **N749** with a DSC sensitized by **73** having the highest power conversion efficiency of 9.21% [62]. In the most recent variation of these complexes, **79**, a quinoline was introduced in place of a pyridine in the tctpy ligand and the efficiency of the device was improved to just above 10% [64].

Complexes **80–84** have 1,2,3-triazoles as parts of a tridentate ligand, Fig. 25. Due to the electronic character of a triazole compared to a pyrazole, electron withdrawing groups such as $-CF_3$ are not necessary to have complexes with a suitable oxidation potential. Complex **80** has two anionic triazolate groups and its oxidation potential is 0.86 V *versus* NHE [65]. In complexes **81–83**, neutral 1,2,3-triazoles are used as the flanking units of a cyclometalated phenyl [66]. The absorption spectra are blue shifted compared to **N749**, with minor differences among the three complexes. DSCs made with these complexes have much lower power conversion efficiencies than devices made with **N749** mainly due to a much lower photocurrent [65,66].

Complex **84** is a unique design where phosphonic acid substituents on the tridentate ligand away from the TiO2 surface are used to achieve robust anchoring of the dye on titania in aqueous media [67].

6. Conclusion

Ruthenium complexes have been studied as sensitizers for dye-sensitized solar cells for more than a decade. A variety of molecular designs have been developed and they have championed the field with devices demonstrating power conversion efficiencies above 10% [68,69].

In this review we have focused on ruthenium complexes with tridentate ligands from a chemical structure perspective and we have not entered the details of the device performance. Since the report about **N749**, the "black dye" $RuL(NCS)_3$ with L = 4,4′,4″-tricarboxylate-2,2′:6′,2″-terpyridine (tctpy), these complexes have attracted attention due to the possibility to harvest near infrared photons. Driven by this property, early examples have focused on red shifting the absorption, and sensitization up to 1000 nm has been demonstrated. However the performances of the devices were generally found to be low because of poorly suited energy levels, in particular because of low lying π^* orbitals strongly limiting the electron injection efficiency. When the energy levels are properly tuned, power conversion efficiencies in excess of that obtained with **N749** have been achieved. Key data for selected sensitizers leading to high efficiency devices are summarized in Table 1.

Due to the distorted geometry induced by the tridentate ligand around the ruthenium center, the excited state relaxation to the ground state is fast and competes with the injection process. Because of this, a large driving force for injection is necessary, which is detrimental to the overall efficiency of the device.

The use of the iodide/triodide redox mediator ultimately limits the possibility of harvesting photons in the near infrared. The advent of finely tunable redox shuttle systems will lift this constraint. Further improvement will be achieved by developing chemical designs leading to efficient injection without the necessity of a high driving force.

Acknowledgments

The authors acknowledge the European Union (HetIridium, Grant CIG322280), for financial support (EB) and the School of Chemistry, University of Birmingham, for a studentship, and the EPSRC for underpinning support (TWR).

References

[1] M.J. de Wild.-Scholten. A.C. Veltkamp, in: Proceedings of Renewable Energy Conference, Makuhari, chiba, Japan, 2006.
[2] K. Okada, H. Matsui, N. Tanabe, Fujikura Tech. Rev. (2012) 27.
[3] B. O'Regan, M. Grätzel, Nature 353 (1991) 737.
[4] A. Hagfeldt, G. Boschloo, L. Sun, L. Kloo, H. Pettersson, Chem. Rev. 110 (2010) 6595.
[5] M.K. Nazeeruddin, E. Baranoff, M. Grätzel, Sol. Energy 85 (2011) 1172.

[6] M.K. Nazeeruddin, F. De Angelis, S. Fantacci, A. Selloni, G. Viscardi, P. Liska, S. Ito, B. Takeru, M. Gratzel, J. Am. Chem. Soc. 127 (2005) 16835.
[7] B. Bozic-Weber, E.C. Constable, C.E. Housecroft, Coord. Chem. Rev. 257 (2013) 3089.
[8] M.E. Ragoussi, M. Ince, T. Torres, Eur. J. Org. Chem. 2013 (2013) 6475.
[9] L.L. Li, E.W. Diau, Chem. Soc. Rev. 42 (2013) 291.
[10] S. Ferrere, B.A. Gregg, J. Am. Chem. Soc. 120 (1998) 843.
[11] T. Bessho, E.C. Constable, M. Grätzel, A. Hernandez Redondo, C.E. Housecroft, W. Kylberg, M.K. Nazeeruddin, M. Neuburger, S. Schaffner, Chem. Commun. (2008) 3717.
[12] E. Baranoff, J.H. Yum, I. Jung, R. Vulcano, M. Grätzel, M.K. Nazeeruddin, Chem. Asian J. 5 (2010) 496.
[13] E.C. Constable, A. Hernandez Redondo, C.E. Housecroft, M. Neuburger, S. Schaffner, Dalton Trans. (2009) 6634.
[14] C.L. Linfoot, P. Richardson, T.E. Hewat, O. Moudam, M.M. Forde, A. Collins, F. White, N. Robertson, Dalton Trans. 39 (2010) 8945.
[15] Y.J. Yuan, Z.T. Yu, J.Y. Zhang, Z.G. Zou, Dalton Trans. 41 (2012) 9594.
[16] T.E. Hewat, L.J. Yellowlees, N. Robertson, Dalton Trans. 43 (2014) 4127.
[17] M.K. Nazeeruddin, A. Kay, I. Rodicio, R. Humphry-Baker, E. Mueller, P. Liska, N. Vlachopoulos, M. Grätzel, J. Am. Chem. Soc. 115 (1993) 6382.
[18] M.K. Nazeeruddin, S.M. Zakeeruddin, R. Humphry-Baker, M. Jirousek, P. Liska, N. Vlachopoulos, V. Shklover, C.H. Fischer, M. Gratzel, Inorg. Chem. 38 (1999) 6298.
[19] S. Campagna, F. Puntoriero, F. Nastasi, G. Bergamini, V. Balzani, Photochemistry and photophysics of coordination compounds: Ruthenium, in: V. Balzani, S. Campagna (Eds.), Photochemistry and Photophysics of Coordination Compounds I, 2007, p. 117.
[20] M.K. Nazeeruddin, P. Pechy, T. Renouard, S.M. Zakeeruddin, R. Humphry-Baker, P. Comte, P. Liska, L. Cevey, E. Costa, V. Shklover, L. Spiccia, G.B. Deacon, C.A. Bignozzi, M. Grätzel, J. Am. Chem. Soc. 123 (2001) 1613.
[21] Y. Chiba, A. Islam, Y. Watanabe, R. Komiya, N. Koide, L.Y. Han, Jpn. J. Appl. Phys. 2 (45) (2006) L638.
[22] L.Y. Han, A. Islam, H. Chen, C. Malapaka, B. Chiranjeevi, S.F. Zhang, X.D. Yang, M. Yanagida, Environ. Sci. 5 (2012) 6057.
[23] S. Fantacci, M.G. Lobello, F. De Angelis, Chimia 67 (2013) 121.
[24] R. Katoh, A. Furube, N. Fuke, A. Fukui, N. Koide, J. Phys. Chem. C 116 (2012) 22301.
[25] Z.S. Wang, C.H. Huang, Y.Y. Huang, B.W. Zhang, P.H. Xie, Y.J. Hou, K. Ibrahim, H.J. Qian, F.Q. Liu, Sol. Energy Mater. Sol. Cells 71 (2002) 261.
[26] T. Funaki, M. Yanagida, N. Onozawa-Komatsuzaki, Y. Kawanishi, K. Kasuga, H. Sugihara, Sol. Energy Mater. Sol. Cells 93 (2009) 729.
[27] G.C. Vougioukalakis, T. Stergiopoulos, G. Kantonis, A.G. Kontos, K. Papadopoulos, A. Stublla, P.G. Potvin, P. Falaras, J. Photochem. Photobiol. A 214 (2010) 22.
[28] N. Onozawa-Komatsuzaki, M. Yanagida, T. Funaki, K. Kasuga, K. Sayama, H. Sugihara, Inorg. Chem. Commun. 12 (2009) 1212.
[29] N. Onozawa-Komatsuzaki, M. Yanagida, T. Funaki, K. Kasuga, K. Sayama, H. Sugihara, Sol. Energy Mater. Sol. Cells 95 (2011) 310.
[30] N. Onozawa-Komatsuzaki, T. Funaki, K. Kasuga, Y. Nakazawa, K. Sayama, H. Sugihara, Jpn. J. Appl. Phys. 51 (2012).
[31] K. Chen, Y.H. Hong, Y. Chi, W.H. Liu, B.S. Chen, P.T. Chou, J. Mater. Chem. 19 (2009) 5329.
[32] F. De Angelis, S. Fantacci, A. Selloni, M.K. Nazeeruddin, M. Grätzel, J. Phys. Chem. C 114 (2010) 6054.
[33] K.S. Finnie, J.R. Bartlet, J.L. Woolfrey, Langmuir 14 (1998) 2744.
[34] S.H. Yang, K.L. Wu, Y. Chi, Y.M. Cheng, P.T. Chou, Angew. Chem., Int. Ed. Engl. 50 (2011) 8270.
[35] H.W. Lin, Y.S. Wang, Z.Y. Huang, Y.M. Lin, C.W. Chen, S.H. Yang, K.L. Wu, Y. Chi, S.H. Liu, P.T. Chou, Phys. Chem. Chem. Phys. 14 (2012) 14190.
[36] M. Kimura, J. Masuo, Y. Tohata, K. Obuchi, N. Masaki, T.N. Murakami, N. Koumura, K. Hara, A. Fukui, R. Yamanaka, S. Mori, Chem. Eur. J. 19 (2013) 1028.
[37] Y. Numata, S.P. Singh, A. Islam, M. Iwamura, A. Imai, K. Nozaki, L.Y. Han, Adv. Funct. Mater. 23 (2013) 1817.
[38] Y. Numata, A. Islam, K. Sodeyama, Z.H. Chen, Y. Tateyama, L.Y. Han, J. Mater. Chem. A 1 (2013) 11033.
[39] A. Islam, H. Sugihara, M. Yanagida, K. Hara, G. Fujihashi, Y. Tachibana, R. Katoh, S. Murata, H. Arakawa, New J. Chem. 26 (2002) 966.
[40] A. Islam, F.A. Chowdhury, Y. Chiba, R. Komiya, N. Fuke, N. Ikeda, K. Nozaki, L.Y. Han, Chem. Mater. 18 (2006) 5178.
[41] S. Gao, A. Islam, Y. Numata, L.Y. Han, Appl. Phys. Exp. 3 (2010).
[42] T. Funaki, M. Yanagida, N. Onozawa-Komatsuzaki, K. Kasuga, Y. Kawanishi, H. Sugihara, Inorg. Chim. Acta 362 (2009) 2519.
[43] T. Funaki, M. Yanagida, N. Onozawa-Komatsuzaki, K. Kasuga, Y. Kawanishi, M. Kurashige, K. Sayama, H. Sugihara, Chem. Commun. 12 (2009) 842.
[44] C. Moorlag, O. Clot, M.O. Wolf, B.O. Patrick, Chem. Commun. (2002) 3028.
[45] T. Funaki, H. Funakoshi, O. Kitao, N. Onozawa-Komatsuzaki, K. Kasuga, K. Sayama, H. Sugihara, Angew. Chem., Int. Ed. Engl. 51 (2012) 7528.
[46] B.S. Chen, K. Chen, Y.H. Hong, W.H. Liu, T.H. Li, C.H. Lai, P.T. Chou, Y. Chi, G.H. Lee, Chem. Commun. (2009) 5844.
[47] K.S. Chen, W.H. Liu, Y.H. Wang, C.H. Lai, P.T. Chou, G.H. Lee, K. Chen, H.Y. Chen, Y. Chi, F.C. Tung, Adv. Funct. Mater. 17 (2007) 2964.
[48] J.J. Kim, H. Choi, S. Paek, C. Kim, K. Lim, M.J. Ju, H.S. Kang, M.S. Kang, J. Ko, Inorg. Chem. 50 (2011) 11340.
[49] M. Chandrasekharam, G. Rajkumar, C.S. Rao, T. Suresh, Y. Soujanya, P.Y. Reddy, Adv. OptoElectron. 2011 (2011) 1.
[50] L. Giribabu, V.K. Singh, M. Srinivasu, C.V. Kumar, V.G. Reddy, Y. Soujnya, P.Y. Reddy, J. Chem. Sci. 123 (2011) 371.
[51] S.H. Wadman, J.M. Kroon, K. Bakker, M. Lutz, A.L. Spek, G.P. van Klink, G. van Koten, Chem. Commun. (2007) 1907.
[52] S. Caramori, J. Husson, M. Beley, C.A. Bignozzi, R. Argazzi, P.C. Gros, Chem. Eur. J. 16 (2010) 2611.
[53] A. Sepehrifard, S.G. Chen, A. Stublla, P.G. Potvin, S. Morin, Electrochim. Acta 87 (2013) 236.
[54] H.J. Park, K.H. Kim, S.Y. Choi, H.M. Kim, W.I. Lee, Y.K. Kang, Y.K. Chung, Inorg. Chem. 49 (2010) 7340.
[55] S.P. Singh, K.S. Gupta, M. Chandrasekharam, A. Islam, L. Han, S. Yoshikawa, M.A. Haga, M.S. Roy, G.D. Sharma, ACS Appl. Mater. Interfaces 5 (2013) 11623.
[56] S.H. Wadman, J.M. Kroon, K. Bakker, R.W.A. Havenith, G.P.M. van Klink, G. van Koten, Organometallics 29 (2010) 1569.
[57] H. Kisserwan, A. Kamar, T. Shoker, T.H. Ghaddar, Dalton Trans. 41 (2012) 10643.
[58] R.K. Chitumalla, K.S. Gupta, C. Malapaka, R. Fallahpour, A. Islam, L. Han, B. Kotamarthi, S.P. Singh, Phys. Chem. Chem. Phys. 16 (2014) 2630.
[59] H. Kisserwan, T.H. Ghaddar, Dalton Trans. 40 (2011) 3877.
[60] K.C. Robson, B.D. Koivisto, A. Yella, B. Sporinova, M.K. Nazeeruddin, T. Baumgartner, M. Gratzel, C.P. Berlinguette, Inorg. Chem. 50 (2011) 5494.
[61] C.C. Chou, K.L. Wu, Y. Chi, W.P. Hu, S.J. Yu, G.H. Lee, C.L. Lin, P.T. Chou, Angew. Chem., Int. Ed. Engl. 50 (2011) 2054.
[62] K.L. Wu, C.H. Li, Y. Chi, J.N. Clifford, L. Cabau, E. Palomares, Y.M. Cheng, H.A. Pan, P.T. Chou, J. Am. Chem. Soc. 134 (2012) 7488.
[63] C.W. Hsu, S.T. Ho, K.L. Wu, Y. Chi, S.H. Liu, P.T. Chou, Energy Environ. Sci. 5 (2012) 7549.
[64] C.C. Chou, F.C. Hu, H.H. Yeh, H.P. Wu, Y. Chi, J.N. Clifford, E. Palomares, S.H. Liu, P.T. Chou, G.H. Lee, Angew. Chem., Int. Ed. 53 (2014) 178.
[65] S. Sinn, B. Schulze, C. Friebe, D.G. Brown, M. Jäger, J. Kübel, B. Dietzek, C.P. Berlinguette, U.S. Schubert, Inorg. Chem. 53 (2014) 1637.
[66] B. Schulze, D.G. Brown, K.C. Robson, C. Friebe, M. Jäger, E. Birckner, C.P. Berlinguette, U.S. Schubert, Chem. Eur. J. 19 (2013) 14171.
[67] D.G. Brown, P.A. Schauer, J. Borau-Garcia, B.R. Fancy, C.P. Berlinguette, J. Am. Chem. Soc. 135 (2013) 1692.
[68] J.-F. Yin, M. Velayudham, D. Bhattacharya, H.-C. Lin, K.-L. Lu, Coord. Chem. Rev. 256 (2012) 3008.
[69] A. Reynal, E. Palomares, Eur. J. Inorg. Chem. 2011 (2011) 4509.